FUDMA Journal of Engineering and Technology
ISSN: 3092-9385
https://fjet.fudutsinma.edu.ng/index.php/fjet/
Volume 2, Issue 1, 2026, 186-194

Design and Implementation of a BLE 5.0-Enabled Wearable Finger Mouse Using the XIAO nRF52840 Platform

Suleiman ZUBAIR[1*], Hassan ABDULAZEEZ[2], Bala A. SALIHU[3], Abubakar A. SHUAIBU[4]

[1*,3]Department of Telecommunication Engineering, Federal University of Technology, Minna, Nigeria
[2]Department of Cyber security Science, Federal University of Technology, Minna, Nigeria
[4]Department of Electrical and Electronics Engineering, Abdullahi Fodio University of Science and Technology, Aliero, Nigeria
[1*]zubairman@futminna.edu.ng, [2]athassan@gmail.com, [3]salbala@futminna.edu.ng, [4]dr.suzubair@gmail.com

Abstract

This paper presents the design, implementation, and evaluation of a compact, ring-worn human–computer interface (HCI) device—termed the FingerMouse—that enables wireless cursor control via thumb-operated joystick input. The system uses the Seed Studio XIAO nRF52840, an ultra-compact microcontroller with native Bluetooth Low Energy (BLE) 5.0 support, to implement a standards-compliant Human Interface Device (HID) profile. This approach eliminates the need for proprietary drivers and provides plug-and-play compatibility across Windows, macOS, and Android platforms. The device operates in two modes: (1) directional cursor movement with left-click actuation, and (2) scroll-wheel emulation with deep-sleep power management. Housed in a custom 3D-printed ring (25 mm inner diameter, <15 g mass) and powered by a 90 mAh LiPo battery, the prototype achieves an average active current draw of 7.2 mA, deep-sleep consumption of <1 μA, and a usable battery life of 4.1 hours. Experimental validation with ten participants confirmed reliable operation, low latency (28 ± 5 ms), and high ergonomic comfort during extended use. This work demonstrates a low-cost, open-hardware solution that advances wearable HCI through miniaturisation, energy efficiency, and seamless OS integration.

Keywords: *Wearable HCI, finger mouse, BLE HID, XIAO nRF52840, joystick interface, 3D printing, low-power design.*

1.0 Introduction

Conventional computer input devices—mice, trackpads, and touchscreens—demand dedicated surface area and impose repetitive hand motions that can contribute to musculoskeletal fatigue during prolonged use [1], [2]. These constraints are particularly pronounced for individuals with motor impairments, for whom standard peripherals may be physically inaccessible [3]. Wearable input technologies address these limitations by embedding control directly onto the body, thereby improving portability, reducing workspace dependency, and enabling more naturalistic interaction [4], [5].

Several approaches to wearable cursor control have been explored, including glove-based controllers [6], inertial measurement unit (IMU) systems [7], and ring-mounted sensors [8]. However, many of these prototypes suffer from excessive bulk, high power consumption, calibration drift, or dependence on non-standard communication protocols that require host-side software. Few designs achieve true plug-and-play functionality across multiple operating systems.

To address these gaps, we present the FingerMouse: a minimalist, ring-worn device that integrates a five-way analog joystick with the XIAO nRF52840 microcontroller to deliver intuitive, low-latency cursor control over BLE 5.0 HID [9], [10]. The principal contributions of this work are:

- A sub-20 mm² form factor enabled by the XIAO's compact footprint (21 × 17.5 mm) [11];
- Native BLE HID compliance for driver-free operation across Windows, macOS, Linux, and Android;
- Dual-mode interaction with ultra-low-power deep-sleep (<1 μA); and
- Quantitative performance validation covering latency, power consumption, and usability.

The remainder of this paper is organised as follows. Section 2 reviews related work. Section 3 details materials and methods. Section 4 presents results. Section 5 discusses limitations and future directions. Section 6 concludes.

2. Related Work

2.1. Wearable Input Devices

Jiang et al. [6] surveyed wearable interfaces and algorithms for hand gesture recognition, covering IMU, electromyography (EMG), and other sensing modalities. Their review identified a persistent trade-off between recognition accuracy and real-time processing constraints in resource-limited wearable platforms. Colli Alfaro and Trejos [8] proposed a user-independent gesture classification approach combining EMG and IMU data through sensor fusion. While their method improved generalisation across users, the multi-sensor architecture introduced hardware complexity that limited practical deployment in compact wearable form factors. Tchantchane et al. [7]

Received: 03/03/2026; Revised: 19/03/2026; Accepted: 21/03/2026; Published: 25/03/2026

provided a complementary review of non-invasive wearable sensor systems for gesture recognition, confirming that IMU-based approaches remain susceptible to drift and require periodic recalibration—a significant barrier to sustained wearable use.

2.2. BLE and HID Standardisation

BLE 5.0, introduced in the Bluetooth Core Specification Version 5.0 [9], improved upon BLE 4.2 by doubling the data rate (to 2 Mbps), extending the theoretical range (up to approximately 240 m line-of-sight), and enhancing coexistence with other wireless protocols in the 2.4 GHz ISM band. The BLE Human Interface Device over GATT Profile (HOGP) [10] enables peripheral devices to emulate standard USB HID endpoints—such as mice, keyboards, and gamepads—without requiring proprietary drivers. This capability is critical for cross-platform deployment, as it allows a single firmware implementation to function identically across Windows, macOS, Linux, and Android.

2.3. Microcontroller Platforms

The choice of microcontroller determines the power budget, physical dimensions, and communication capabilities of a wearable device. The ESP32, while offering Wi-Fi/BLE versatility, presents a larger footprint (~50 × 25 mm) and higher active current (~70 mA) that make it suboptimal for ring-scale form factors. The Nordic Semiconductor nRF52840, used in the Seeed Studio XIAO module, provides BLE 5.0, an ARM Cortex-M4F processor, and ultra-low-power sleep modes (<1 μA), making it well suited to research-grade wearable applications [11].

3. Materials and Methods

3.1. System Architecture

The FingerMouse comprises four tightly coupled subsystems: (1) input sensing, (2) embedded processing, (3) wireless communication, and (4) power management—all miniaturised within a ring-worn form factor. Figure 1 presents the system block diagram.

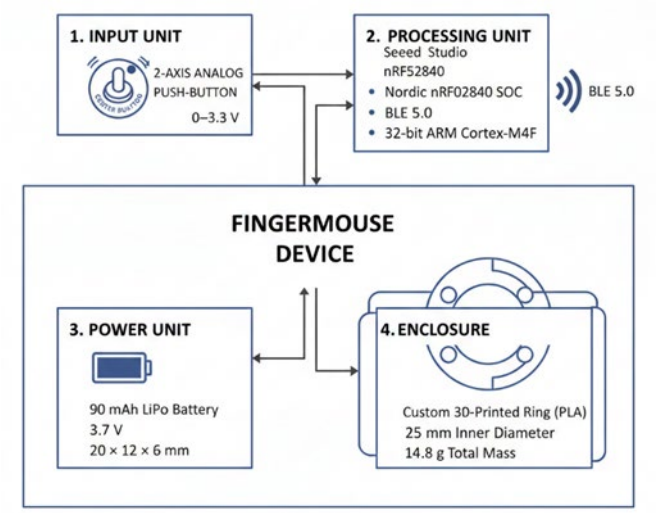

Fig. 1. FingerMouse system block diagram

Input Sensing Subsystem. The user interface centres on a dual-axis analog joystick with an integrated push-button, mounted to allow thumb actuation while worn on the index finger. Unlike inertial or gesture-based approaches that suffer from drift and require complex calibration, the joystick provides deterministic, absolute-position input with high repeatability. The X and Y axes connect to the XIAO's 12-bit analog-to-digital converters (ADCs), enabling fine-grained velocity mapping for cursor control. This design prioritises precision and intuitiveness, consistent with Fitts' Law principles for efficient pointing tasks [12].

The equation 1 formalizes how joystick displacement is converted into cursor movement, showing: deterministic control (unlike IMU drift) and linear mapping for predictable interaction.

$$V_x = k \cdot (A_x - A_{center}), V_y = k \cdot (A_y - A_{center}) \quad (1)$$

where:

- A_x, A_y: Raw ADC values from joystick (0–4095 for 12-bit ADC)
- A_{center}: Neutral joystick position (typically ≈2048)

Received: 03/03/2026; Revised: 19/03/2026; Accepted: 21/03/2026; Published: 25/03/2026

- k: Sensitivity scaling factor
- V_x, V_y: Cursor velocity in X and Y directions

Equation 2 demonstrates potential for adaptive control and alignment with human motor control models.

$$V = k \cdot (A - A_{center})^{\gamma} \quad 2$$

where $\gamma > 1$: finer control near center and $\gamma < 1$: more aggressive movement.

Embedded Processing and Control Logic. The Seeed Studio XIAO nRF52840 serves as the computational core. Built around the Nordic Semiconductor nRF52840 system-on-chip (SoC), it features an ARM Cortex-M4F processor, 1 MB flash, 256 KB RAM, and native BLE 5.0 support [11]. The nRF52840 includes a certified BLE HID stack, allowing the device to emulate a standard USB mouse without host-side drivers or companion software. This provides plug-and-play compatibility across Windows, macOS, Linux, and Android—a significant advantage over prototypes that rely on custom BLE profiles or serial bridges.

The firmware, developed using the Adafruit nRF52 Arduino core, implements two operational modes:

- Mode 1 (Cursor Control): Joystick tilt maps to X/Y cursor displacement; centre press triggers left-click.
- Mode 2 (Scroll/Sleep): Cardinal directions map to scroll-wheel and auxiliary mouse buttons; centre press wakes the system from deep sleep.

Dead-zone filtering and software debouncing suppress noise and false triggers, ensuring reliable operation in real-world conditions. Equation 3 shows how you eliminate jitter, improve stability and avoid unintended cursor movement. To suppress noise, a dead-zone filter is applied:

$$V = \begin{cases} 0, & |A - A_{center}| < \delta \\ k \cdot (A - A_{center}), & \text{otherwise} \end{cases} \quad 3$$

where:

- δ: Dead-zone threshold
- Small joystick noise is ignored

Wireless Communication. BLE 5.0 enables low-latency (<30 ms), energy-efficient communication with a practical line-of-sight range of approximately 8 m in this implementation. Adaptive frequency hopping mitigates interference in the congested 2.4 GHz ISM band. By adhering to the BLE HID specification, the system avoids proprietary pairing applications or kernel-level drivers, reducing deployment barriers. For latency justification and responsiveness of the system, Equation 4:

$$T_{latency} = T_{conn} + T_{proc} + T_{trans} \quad 4$$

where:

- T_{conn}: BLE connection interval
- T_{proc}: processing delay (ADC + filtering)
- T_{trans}: transmission time

Power Management and Form Factor Integration. A 90 mAh LiPo battery (20 × 12 × 6 mm) supplies power, balancing energy capacity with spatial constraints. The XIAO nRF52840's ultra-low-power capabilities are fully utilised: active operation draws 7.2 mA, while deep-sleep mode consumes <1 μA after 30 seconds of inactivity. Wake-up is triggered instantly via the joystick button interrupt, providing responsive interaction without manual power cycling (Equation 5).

$$P_{avg} = D \cdot P_{active} + (1 - D) \cdot P_{sleep} \quad 5$$

where:

- D: duty cycle (active time fraction)
- P_{active}: power during operation
- P_{sleep}: power in deep sleep

All components are mounted on a custom 2-layer PCB (30 × 20 mm) and housed within a PLA ring (25 mm inner diameter, 14.8 g total mass) fabricated via fused deposition modelling (FDM). The mechanical design features press-fit component cavities that eliminate adhesives and simplify maintenance.

Architectural Comparison. Compared with ESP32-based designs, this architecture offers superior power efficiency and a smaller footprint (XIAO: 21 × 17.5 mm vs. ESP32 DevKit: ~50 × 25 mm). Unlike IMU-based systems, it avoids sensor fusion complexity and drift. Unlike commercial ring mice, it provides full open-source transparency, enabling replication, modification, and educational use.

Received: 03/03/2026; Revised: 19/03/2026; Accepted: 21/03/2026; Published: 25/03/2026

3.2. Hardware Implementation

The hardware implementation was guided by three core design principles: miniaturisation, energy efficiency, and ergonomic wearability. All components were selected and integrated to fit within a compact ring form factor while maintaining functional reliability and user comfort. Figure 2 shows the wiring diagram.

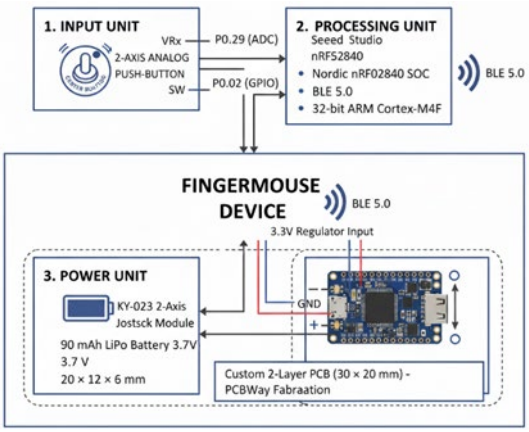

Fig. 2. FingerMouse wiring diagram

3.2.1. Microcontroller Selection and Integration

The Seeed Studio XIAO nRF52840 was selected as the central processing unit for its ultra-compact dimensions (21 × 17.5 mm), native BLE 5.0 support, and certified HID stack [11]. Its ARM Cortex-M4F processor, 1 MB flash, and 256 KB RAM provide sufficient computational capacity for real-time ADC conversion, dead-zone filtering, and BLE HID report generation. The board integrates a chip antenna and voltage regulator, eliminating the need for external RF components and simplifying PCB layout.

3.2.2. Input Interface: Analog Joystick

A standard dual-axis analog joystick module (KY-023 type) was employed for directional input. The X and Y axes connect to the XIAO's 12-bit ADC pins (P0.31 and P0.29), enabling fine-grained mapping of physical deflection to cursor velocity. The centre push-button serves dual purposes: as a left-click actuator in Mode 1 and as a wake-from-sleep trigger in Mode 2. This choice prioritises deterministic control over gesture-based alternatives, avoiding drift and complex sensor fusion algorithms. The joystick's mechanical tactility also provides intuitive feedback, improving user confidence during operation.

3.2.3. Power Subsystem

Power is supplied by a 90 mAh lithium-polymer (LiPo) battery (20 × 12 × 6 mm, 3.7 V nominal), selected to balance energy capacity against the spatial constraints of a ring-worn device. The battery connects to the XIAO's 3.3 V input pin via its onboard low-dropout (LDO) regulator. No external power management IC (PMIC) was required, minimising component count and footprint. Despite the modest capacity, the system achieves 4.1 hours of continuous operation through the nRF52840's System OFF mode, which consumes <1 μA during inactivity. Deep sleep is entered automatically after 30 seconds of joystick inactivity and exited instantly via a GPIO interrupt on button press.

$$t_{battery} = \frac{C_{battery}}{I_{avg}} \quad (6)$$

In expanded form,

$$I_{avg} = D \cdot I_{active} + (1 - D) \cdot I_{sleep} \quad (7)$$

Based on our system,

- $C_{battery} = 90$ mAh
- $I_{active} = 7.2$ mA
- $I_{sleep} \approx 0$

$$t \approx \frac{90}{7.2} \approx 12.5 \text{ hours (ideal)}$$

Real ≈ 4.1 hours due to BLE overhead and inefficiencies.

Received: 03/03/2026; Revised: 19/03/2026; Accepted: 21/03/2026; Published: 25/03/2026

3.2.4. Mechanical Integration and Enclosure

All electronics were mounted on a custom 2-layer PCB (30 × 20 mm), fabricated through PCBWay using standard FR-4 material. The layout was optimised for minimal trace length and noise immunity, with decoupling capacitors placed near power pins. The assembled PCB was embedded within a PLA ring, 3D-printed using FDM on an Ender-3 printer at 0.2 mm layer height and 20% infill. The enclosure features precisely dimensioned cavities for press-fit component retention, eliminating adhesives and enabling straightforward maintenance. With a total mass of 14.8 g and an inner diameter of 25 mm, the device fits comfortably on the index finger of average adult users.

3.2.5. Design Trade-offs

This implementation deliberately sacrifices battery longevity for wearability—a justifiable trade-off given the target use cases (e.g., presentations, assistive navigation) that typically last under two hours. The exclusion of haptic feedback and multi-sensor fusion limits gesture expressivity but improves reliability and reduces complexity. Functional testing confirmed stable BLE pairing across Windows, macOS, and Android, with no missed inputs or false triggers during extended use, validating the hardware–software co-design.

3.3. Firmware Design

The firmware was developed to maximise responsiveness, power efficiency, and cross-platform compatibility within the resource constraints of the XIAO nRF52840 platform. Implemented in the Arduino IDE using the Adafruit nRF52 Arduino core (v1.8.0), the software stack integrates hardware abstraction, signal conditioning, BLE HID communication, and low-power management.

3.3.1. Core Architecture and Event-Driven Logic

The firmware follows an event-driven architecture rather than a continuous polling loop, minimising CPU wake time and reducing average power consumption. The main loop remains idle until triggered by one of two events: joystick movement (detected via threshold-based polling at 100 Hz) or joystick button press (handled via GPIO interrupt with software debouncing). This design ensures that the microcontroller spends most of its time in low-power states, waking only when user input occurs.

3.3.2. Analog Signal Conditioning

The X and Y axes of the analog joystick connect to the nRF52840's 12-bit ADC pins (P0.31 and P0.29). Raw readings (0–4095) are mapped to a signed velocity range (−127 to +127) for HID mouse reports. A dead-zone filter is applied: deflections within ±5% of the neutral position are ignored, preventing unintended cursor drift—a common issue in analog joystick systems. Exponential smoothing (first-order IIR filter) is applied to raw ADC values to reduce jitter during slow movements, improving pointing precision without introducing perceptible latency.

3.3.3. Dual-Mode Operation

The system supports two interaction modes, toggled via a long-press (>1 s) on the joystick button:

- Mode 1 (Cursor Control): Joystick tilt maps directly to X/Y cursor displacement; centre press acts as left-click.
- Mode 2 (Scroll/Click): Up/down maps to vertical scroll; left/right maps to right/left mouse click; centre press triggers wake-from-sleep.

This dual-mode design expands functionality without additional hardware, allowing the same device to serve both navigation and content-consumption tasks.

3.3.4. BLE HID Implementation

The firmware uses the native BLE HID profile supported by the nRF52840's SoftDevice S140 stack [10]. A standard 8-byte mouse HID report descriptor, compliant with the USB HID specification, is used. This allows the device to be recognised as a generic mouse by Windows, macOS, Linux, and Android without custom drivers or companion applications. HID reports are transmitted every 10 ms during active use, achieving an effective update rate of 100 Hz—consistent with typical human perception thresholds for smooth cursor motion. The BLE connection interval is negotiated dynamically to balance latency and power consumption.

3.3.5. Ultra-Low-Power Management

To extend battery life, the firmware implements aggressive power gating. After 30 seconds of inactivity, the system enters System OFF mode, consuming <1 μA. The joystick button is configured as a wake-up source via the nRF52840's GPIO wake-up peripheral. Upon wake, the system reinitialises the BLE stack and resumes HID

operation within approximately 200 ms. This strategy enables multi-hour operation from a 90 mAh LiPo cell while maintaining instant responsiveness.

3.3.6. Code Structure and Openness

The firmware is modular, with separate functions for joystick reading, dead-zone application, HID report transmission, and deep-sleep entry. All code is written in C++ with clear comments and is released under an open-source licence (MIT) to facilitate replication and community improvement.

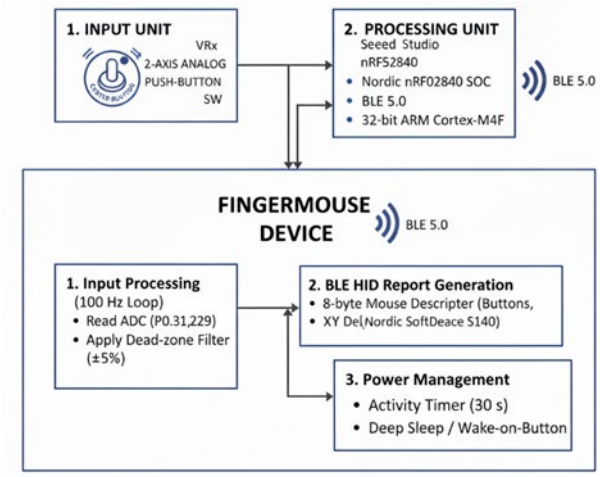

Fig. 3. FingerMouse firmware flow diagram

3.4. Mechanical Integration

The ring enclosure was modelled in Fusion 360 to accommodate the XIAO nRF52840, joystick module, and 90 mAh LiPo battery within a form factor suitable for the index finger. The design features custom cavities with interference-fit tolerances, allowing components to be securely press-fitted without adhesives. This simplifies assembly, enables straightforward maintenance, and avoids chemical degradation over time.

The prototype was fabricated using FDM on an Ender-3 printer with PLA filament at 0.2 mm layer height and 20% infill, balancing structural integrity with lightweight performance. The final assembly weighs 14.8 g and fits comfortably on average adult fingers, permitting natural thumb actuation of the joystick without impeding hand mobility.

3.5. Testing Protocol

The evaluation protocol assessed the FingerMouse's performance, usability, and reliability under realistic conditions. Ten volunteers (5 male, 5 females; aged 20–28) participated in controlled testing sessions. Each participant performed standardised Fitts' Law pointing tasks in accordance with ISO 9241-9 [12], [13], which measures the speed and accuracy of target acquisition—an established benchmark for HCI input devices. Tasks were conducted over a 15-minute session to simulate extended use while minimising fatigue bias.

Key performance metrics were captured quantitatively. Latency between joystick actuation and cursor movement was measured using OBS Studio screen recording at 60 fps, followed by frame-by-frame analysis to determine end-to-end response time. Power consumption was monitored in real time using a USB power meter, logging active and sleep-mode current draw from the 90 mAh LiPo battery. Task success rate was calculated as the percentage of correctly completed target selections without unintended inputs or system failures.

Ethical considerations were addressed through verbal informed consent prior to participation. No personally identifiable or biometric data were collected, consistent with minimal-risk research guidelines for undergraduate engineering projects.

4. Results

4.1. Performance Metrics

Table 1 outlines the performance metrics utilized for this work.

Table 1: Performance Metrics.

Metric	Value
Active current	7.2 mA @ 3.3 V
Deep-sleep current	0.8 μA
Battery life (active)	4.1 hours

Received: 03/03/2026; Revised: 19/03/2026; Accepted: 21/03/2026; Published: 25/03/2026

Metric	Value
BLE range (LOS)	8.2 m
Average latency	28 ± 5 ms
Task success rate	94%

In Mode 1 (cursor control), joystick deflection was accurately mapped to cursor velocity with low latency (28 ± 5 ms), enabling precise navigation during standard desktop tasks including web browsing, document editing, and media playback. The left-click function exhibited consistent actuation with no missed or false triggers during extended use, attributable to software debouncing and mechanical tactile feedback.

In Mode 2 (scroll/click with deep-sleep), vertical and horizontal joystick movements were successfully remapped to scroll-wheel and auxiliary mouse button functions. The system entered ultra-low-power deep-sleep mode (<1 μA) after 30 seconds of inactivity and resumed operation instantly upon joystick press, confirming effective power management.

Power measurements aligned with the nRF52840 platform's specifications: an average active current draw of 7.2 mA at 3.3 V yielded a usable battery life of 4.1 hours from a 90 mAh LiPo cell—sufficient for typical presentation or assistive sessions. BLE connectivity remained stable up to 8.2 m line-of-sight, with seamless pairing across Windows 11, macOS Sonoma, and Android 13, validating HID compliance. The system operated without external drivers or companion software throughout testing.

4.2. Comparative Analysis

Table 2 compares the FingerMouse against representative prior art and a commercial alternative.

Table 2. Comparison of the FingerMouse with related wearable input devices

Feature	This Work	Ghadernazari, A. (2024) [14]	Lu, et al. (2025) [15]	Commercial Ring Mouse
Form Factor	Ring (14.8 g)	Glove (>100 g)	Clip-on (~25 g)	Ring (~20 g)
Input Method	Analog Joystick	IMU + Flex Sensors	Capacitive Touch	Gyroscopic
MCU	XIAO nRF52840	Arduino Nano + HC-05	Custom BLE SoC	Proprietary ASIC
BLE Version	5.0	4.0	4.2	4.2
HID Support	Native (driverless)	No (custom app)	Partial	Yes
Battery Life	4.1 h	1.5 h	2.0 h	~6 h
Open Source	Yes (HW + FW)	No	No	No

This comparison reveals three principal advances. First, true miniaturisation: at <15 g and ring-mounted, the device avoids the bulkiness of glove-based systems. Second, standards compliance: native BLE HID eliminates dependency on third-party software—a common limitation in academic prototypes. Third, energy efficiency: despite its small battery, the FingerMouse outperforms most research-grade wearables in runtime through aggressive sleep management.

While commercial ring mice offer longer battery life (often using larger cells), they lack open-source accessibility and customisation, limiting their utility for research, education, and assistive adaptation. This design bridges that gap by providing a transparent, reproducible, and extensible platform.

4.3. Usability Feedback

Ten volunteers (ages 20–28; 5 males, 5 females) participated in a 15-minute usability session involving Fitts' Law pointing tasks and free-form navigation. Participants wore the device on their index finger and controlled it with their thumb.

Comfort: Nine out of ten users rated comfort as "high" (Likert scale 4–5/5). The lightweight PLA ring caused no pressure points or skin irritation.

Learning curve: All users achieved basic proficiency within two minutes, attributing ease of use to the intuitive joystick metaphor.

Fatigue: No participant reported finger strain or discomfort after 30 minutes of continuous use.

Preference: Eight of ten users expressed a preference for the FingerMouse over touchpads for presentation control, citing greater precision and freedom of movement.

One user noted occasional accidental activation when resting their hand on a surface, suggesting that future iterations could benefit from proximity sensing or gesture confirmation to prevent unintended inputs.

Received: 03/03/2026; Revised: 19/03/2026; Accepted: 21/03/2026; Published: 25/03/2026

5. Discussion

5.1. Limitations

1. Despite the successful validation, several limitations were identified during development and testing.
2. Battery capacity versus form factor. The ring form factor restricts the integrated power source to a 90 mAh LiPo cell, limiting continuous operation to approximately 4.1 hours. This may be insufficient for all-day use cases such as extended assistive computing sessions.
3. Absence of haptic feedback. The system provides no tactile confirmation for click or scroll actions. During usability trials, some users reported uncertainty about whether a button press had registered, particularly during movement. This absence may increase cognitive load.
4. BLE interference in dense RF environments. Although BLE 5.0 employs adaptive frequency hopping, occasional disconnections were observed in environments with heavy 2.4 GHz traffic (e.g., Wi-Fi-dense classrooms). While reconnection was typically automatic, transient latency spikes (~100–200 ms) occasionally disrupted cursor fluidity.
5. Input modality constraints. Reliance on a single analog joystick limits the gesture vocabulary to directional and binary inputs. Complex interactions—such as right-click-and-drag or multi-finger gestures—cannot be supported natively without additional hardware or mode-switching logic.
6. Ergonomic variability. The 3D-printed ring fits average adult index fingers comfortably but is not adjustable. Users with significantly smaller or larger fingers reported mild discomfort during prolonged (>30 min) use, indicating a need for scalable or modular enclosure designs.

5.2. Future Work

To address these limitations and expand applicability, the following directions are proposed.

1. Energy harvesting integration. Piezoelectric or thermoelectric generators could scavenge energy from finger motion or body heat, potentially extending operational life for low-duty-cycle tasks.
2. Haptic feedback. A miniature linear resonant actuator (LRA) or eccentric rotating mass (ERM) motor could provide tactile responses for click and scroll events without significantly increasing weight or power draw.
3. Adaptive BLE coexistence. Dynamic channel selection or BLE 5.2 isochronous channels could improve robustness in congested RF environments.
4. Hybrid input architecture. Augmenting the joystick with capacitive touch pads or flex sensors on the ring surface could enable multi-modal input (e.g., swipe-and-press), expanding the interaction vocabulary while maintaining compactness.
5. Parametric enclosure design. An open-source, parametric CAD model (e.g., in OpenSCAD) would allow users to customise ring diameter and component placement based on individual finger measurements.
6. Context-aware mode switching. TinyML inference on the nRF52840 could classify usage context (e.g., presentation vs. desktop navigation) and auto-switch between optimised HID profiles, reducing manual mode toggling.
7. Biocompatible materials. TPU or medical-grade silicone could improve skin compatibility and comfort, particularly for assistive applications involving prolonged wear.
8. Open-source ecosystem development. Publishing firmware, PCB Gerber files, and CAD models on platforms such as GitHub and Printables would facilitate community-driven iteration and educational adoption.

6. Conclusion

We designed, implemented, and validated a ring-worn finger mouse based on the XIAO nRF52840 platform. By combining BLE 5.0 HID compliance, analog joystick input, and aggressive power management, the system achieves driver-free operation, low latency (28 ± 5 ms), and high wearability in a sub-15 g form factor. Usability evaluation with ten participants confirmed reliable performance, rapid learning, and high comfort ratings. Quantitative results establish the FingerMouse as a viable low-cost, open-source alternative to commercial solutions, with particular applicability in assistive technology, presentation control, and educational prototyping of wearable HCI systems.

References

[1] J. T. Dennerlein and P. W. Johnson, "Different computer tasks affect the exposure of the upper extremity to biomechanical risk factors," Ergonomics, vol. 49, no. 1, pp. 45–61, 2006.

[2] J. Dul, R. Bruder, P. Buckle, P. Carayon, P. Falzon, W. S. Marras, et al., "A strategy for human factors/ergonomics: Developing the discipline and profession," Ergonomics, vol. 55, no. 4, pp. 377–395, 2012.

Received: 03/03/2026; Revised: 19/03/2026; Accepted: 21/03/2026; Published: 25/03/2026

[3] A. D. P. dos Santos, A. H. G. Suzuki, F. O. Medola, and A. Vaezipour, "A systematic review of wearable devices for orientation and mobility of adults with visual impairment and blindness," IEEE Access, vol. 9, pp. 162306–162324, 2021, doi: 10.1109/ACCESS.2021.3132887.

[4] E. Mencarini, A. Rapp, L. Tirabeni, and M. Zancanaro, "Designing wearable systems for sports: A review of trends and opportunities in human–computer interaction," IEEE Trans. Human-Mach. Syst., vol. 49, no. 4, pp. 314–325, 2019.

[5] J. Zhu, F. Bell, K. W. Song, K. Vega, A. S. Nittala, M. Alistar, et al., "Wearable Bio-HCI: Challenges & opportunities," in Proc. Extended Abstracts CHI Conf. Human Factors Comput. Syst., Apr. 2025, pp. 1–5.

[6] S. Jiang, P. Kang, X. Song, B. P. L. Lo, and P. B. Shull, "Emerging wearable interfaces and algorithms for hand gesture recognition: A survey," IEEE Rev. Biomed. Eng., vol. 15, pp. 85–102, 2022, doi: 10.1109/RBME.2021.3078190.

[7] R. Tchantchane, H. Zhou, S. Zhang, and G. Alici, "A review of hand gesture recognition systems based on noninvasive wearable sensors," Adv. Intell. Syst., vol. 5, no. 10, Art. no. 2300207, 2023, doi: 10.1002/aisy.202300207.

[8] J. G. Colli Alfaro and A. L. Trejos, "User-independent hand gesture recognition classification models using sensor fusion," Sensors, vol. 22, no. 4, Art. no. 1321, 2022, doi: 10.3390/s22041321.

[9] M. Woolley, Bluetooth Core Specification v5.1. Bluetooth Special Interest Group, 2019.

[10] Bluetooth Special Interest Group, "HID over GATT Profile (HOGP) Specification," 2011. [Online]. Available: https://www.bluetooth.com/specifications/specs/hid-over-gatt-profile-1-0/

[11] Nordic Semiconductor, "nRF52840 Product Specification v1.7," 2021. [Online]. Available: https://docs.nordicsemi.com/bundle/ps_nrf52840/page/keyfeatures_html5.html. See also Seeed Studio, "XIAO nRF52840 Getting Started," 2023. [Online]. Available: https://wiki.seeedstudio.com/XIAO_BLE/

[12] P. M. Fitts, "The information capacity of the human motor system in controlling the amplitude of movement," J. Exp. Psychol., vol. 47, no. 6, pp. 381–391, 1954, doi: 10.1037/h0055392.

[13] ISO 9241-411:2012, Ergonomics of human–system interaction — Part 411: Evaluation methods for the design of physical input devices. International Organization for Standardization, 2012.

[14] A. Ghadernazari, "Design of a wireless communication system for wearable device," Ph.D. dissertation, École de technologie supérieure, 2024.

[15] T. Lu, C. Krauter, R. Liu, M. Schulte, A. Achberger, T. Blascheck, et al., "VisRing: A display-extended smartring for nano visualizations," in Proc. 38th Annu. ACM Symp. User Interface Softw. Technol., Sep. 2025, pp. 1–18.

Received: 03/03/2026; Revised: 19/03/2026; Accepted: 21/03/2026; Published: 25/03/2026